Geodesy and Geospatial Engineering

VAPOUR

UNIVERSITÉ DU LUXEMBOURG

Luxembourg National Research Fund

On the Application of Multipath Stacking Maps for Improved Severe Weather Tracking and Low-cost Antenna Calibration

Felix Norman Teferle, Addisu Hunegnaw, Hüseyin Duman, Hakki Baltaci, Yohannes G. Ejigu, and Jan Dousa

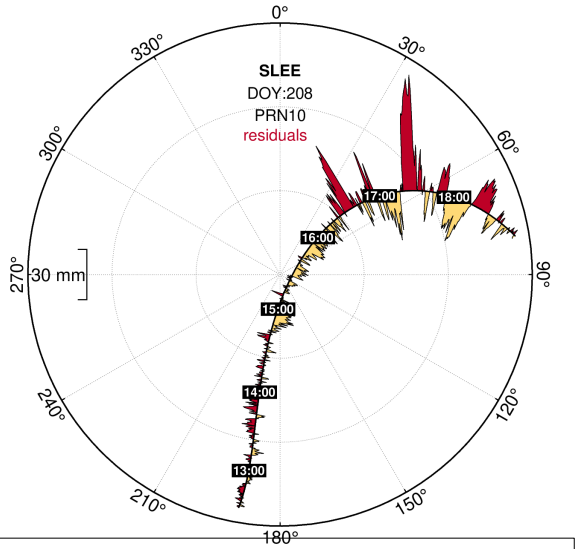

Post-fit residuals during the severe weather

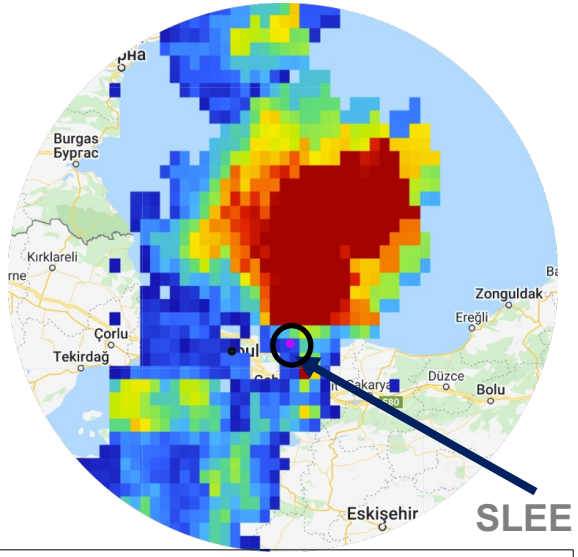

Precipitation 27 July 2017, 17:00 UTC, Turkey

Invited Presentation at the International Summit Forum of Engineering Science and Technology on «Beidou/GNSS Navigation and Location Service in the Intelligent Era», Wuhan, 07 July 2022

Outline

- Motivation and Background
  - The synoptic event of 27 July 2017, Turkey
- Methodology
  - GPS processing and re-constructions of slant delays
  - Multipath stacking maps
  - One-way post-fit residuals
  - Detection of anisotropy in SPWV
- Results
  - Impact of multipath stacking maps
  - Isotropic and non-isotropic components of slant delays
  - Comparison of GPS with ray-traced ERA5 slant delays
- Conclusions

(Ma et al., 2022)
July 20, 2021; sewere weather and subsequent urban flooding in Zhengzhou causes 380 deaths and 41 billion yuan direct economic loss

Severe weather events are predicted to increase in intensity and frequency due to climate change and a better understanding and prediction of these is necessary.

- Slant Wet Delay (SWD) would provide more spatial information on such events than commonly used Zenith Wet Delay (ZWD) and horizontal gradient estimates, but SWD are not operationally assimilated in numerical weather prediction (NWP) models.
- There are at least two reasons for this:
  - SWD estimates require an extra processing step and are estimated as a parametrized form of Zenith Total Delay (ZTD) and the horizontal gradients.
  - **Slant Total Delay (STD) and hence SWD is sensitive to site-specific multipath (MP)**.
- Using Fuhrmann et al. (2015)'s "congruent cells", we developed a MP stacking map from a running average of 21 days of past observations (see AGU FM 2020, EGU21 and EGU22 presentations).
- However, the resulting maps contain the combined effects of MP **and** insufficiently modelled errors, e.g. antenna phase centres.

Synoptic scale circulation that contributed to a severe weather event on 27 July 2017 in Istanbul, Turkey

- During the afternoon hours of July 27, 2017, extreme flash flooding struck Istanbul, Turkey.
- Numerous people were injured, there were several fatalities and severe damage to property and infrastructure.
- Surface temperature of Istanbul reached $34°C$ ($5°C$ above the average)
- A significant amount of moisture was carried by strong southwesterly winds, which resulted from excessive warming of Marmara Sea surface temperatures ($24.9°C$), increasing the convergence of low-level moisture.
- This led to thunderstorms, stormy and gale-force winds (120 km/h) with extreme lightning activity

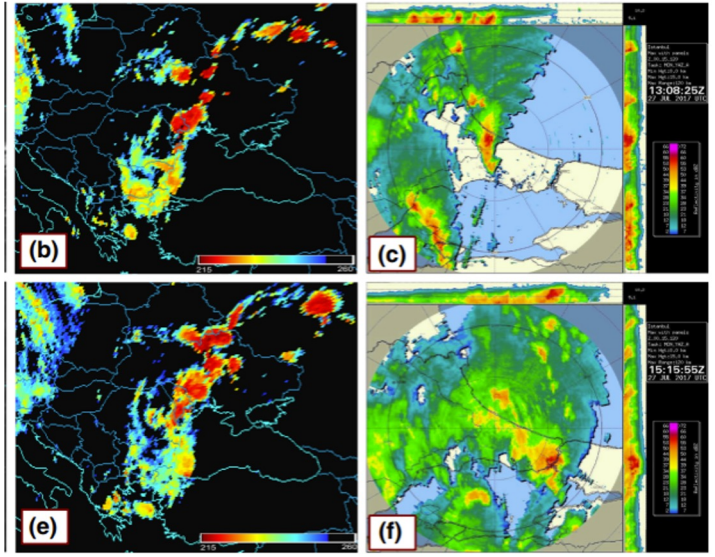

Fig. **b)** 10.8 μm channel of brightness temperature (K) imagery from 13:00 UTC on 27 July 2017. Pixels with brightness temperature K are shown. **c)** Radar MAX product of 13:08 UTC. **e)** and **f)** for 15:15 UTC on 27 July 2017.

The 54 GPS stations that were processed from and around Turkey, with a particular focus on the severe weather event on July 27, 2017.

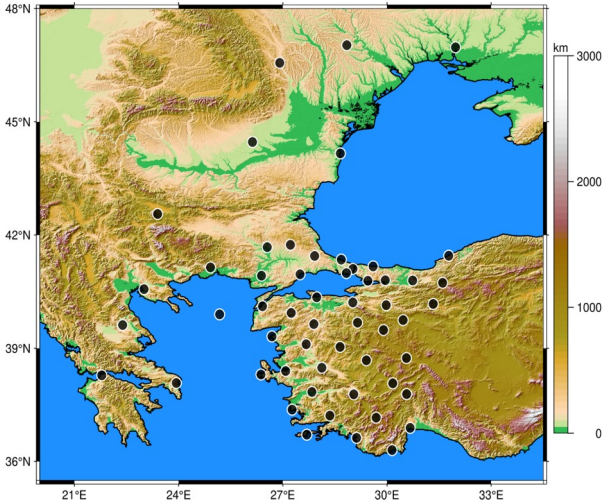

Daily RINEX GPS-only data were processed over a period of 3 months

Processing method:

- PPP by Kalman filtering using JPL-GipsyX GNSS engine
- Estimated parameters:
  - positions (1 XYZ per station) using ITRF14
  - Zenith Tropospheric Delay (epoch-wise)
  - Zenith Wet Delay (ZWD) (epoch-wise)
  - Linear gradients (East, North, epoch-wise)
  - Ambiguity
  - Constraints on ZWD and gradients using RW processes at $10\ \mathrm{mm} \cdot \mathrm{h}^{-1/2}$ & $1.0\ \mathrm{mm} \cdot \mathrm{h}^{-1/2}$

Products:

- Satellite orbit and clock products from JPL
- Ionosphere-free linear combination at 30s intervall and 5-degree elevation cut-off
- Satellite and receiver type-mean PCV/PCOs
- VMF1GRID for tropospheric delay modelling
- High-order ionosphere corrections applied

Construction of STD from ZTD and gradients with additional corrections for residuals and MP.

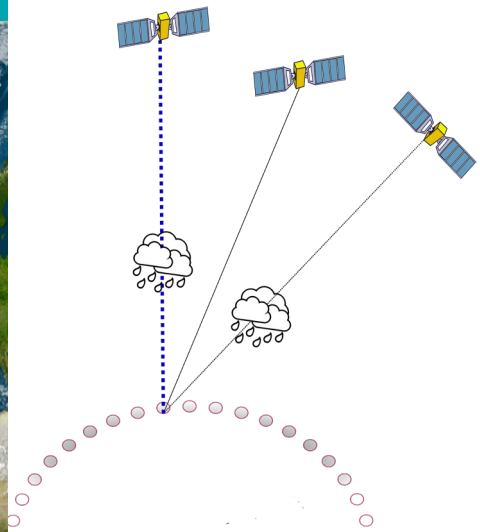

$$STD = T_{atm}(e,\alpha) = ZTD \cdot mf(e) + \xi(e,\alpha) \cdot mf_{grd}(e,\alpha)$$

$$STD = T_{atm}(e,\alpha) = ZTD \cdot mf(e) + \xi(e,\alpha) \cdot mf_{grd}(e,\alpha) + residuals(e,\alpha)$$

$$STD = T_{atm}(e,\alpha) = ZTD \cdot mf(e) + \xi(e,\alpha) \cdot mf_{grd}(e,\alpha) + residuals(e,\alpha) - \mathbf{MPS}\ (e,\alpha)$$

The isotropic and non-isotropic components of slant precipitible water vapour (SPWV)

- Neglecting the dry component between station $\boldsymbol{i}$ and satellite $\boldsymbol{m}$, the slant precipitable water vapour (SPWV) can be written as:

$$SPWV_i^m = \frac{1}{\Pi}\left[PWV \cdot mf(e_i^m) + S_i^m\right]$$

- We measure S_i^m by accurately modelling and correcting for clock delays, satellite orbits, hydrostatic delays, the isotropic part and site-specific MP

- Isotropic component of slant water computed from PWV
- S_i^m, represents the non-isotropic component
- S_i^m is zero for a perfectly isotropic atmosphere
- S_i^m is negative when the GNSS signals pass through areas of low water vapour relative to PWV
- S_i^m positive when the GNSS signal passes through areas of high water vapour relative to PWV

Past Studies on MP Stacking Maps (MPS)

Wanninger and May (2000)	Carrier phase multipath calibration of GPS reference stations
Iwabuchi et al. (2004)	Tsukuba GPS dense net campaign observations: comparison of the stacking maps of post-fit phase residuals estimated from three software packages.
Granström C (2006)	Site-dependent effects in high-accuracy applications of GNSS
Bilich and Larson 2007	Mapping the GPS multipath environment using the signal-to-noise ratio (SNR)
Lidberg et al. (2009)	Site-dependent Effects in High-Accuracy Applications of GNSS
Sidorov and Teferle (2013)	Impact of Antenna Phase Centre Calibrations on Position Time Series
Moore et al. (2014)	Empirical modelling of site-specific errors in continuous GPS data
Fuhrmann et al. (2015)	Generating statistically robust multipath stacking maps using congruent cells

How does the construction of congruent cells for MPS maps work?

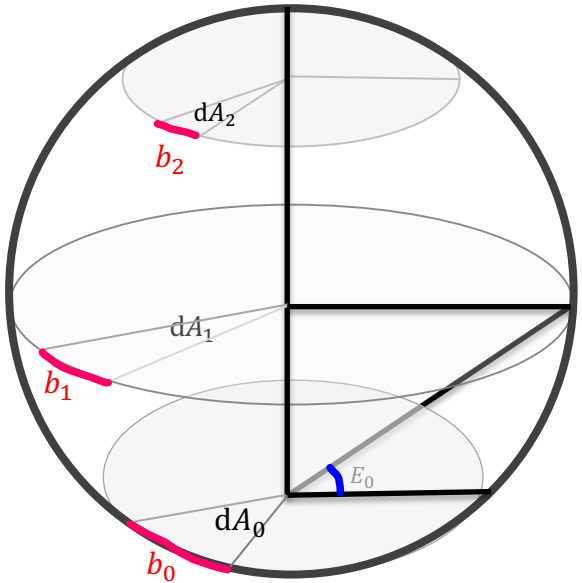

Variable azimuthal resolution, dA_i

Area is kept constant

Horizontal arc lengths are made being equal (b_i), by scaling cosine of elevation angle, for accurately characterizing MP effects for both low and high elevations

Realizing Condition of almost congruence cells with similar shape and size

The site-specific MPS map is generated by computing average of the phase residuals within certain azimuth/elevation interval, i.e. cell. Outliers detected and eliminated with iterative procedure → $3-\sigma$ rule

Courtesy of Fuhrmann, et al. 2015

Post-fit residuals and MPS maps for SARY. Clear site-specific MP is affecting the station. To supress the error, the residuals were averaged for 21 days and the resulting map incorporated to produce non-isotropic slant delay.

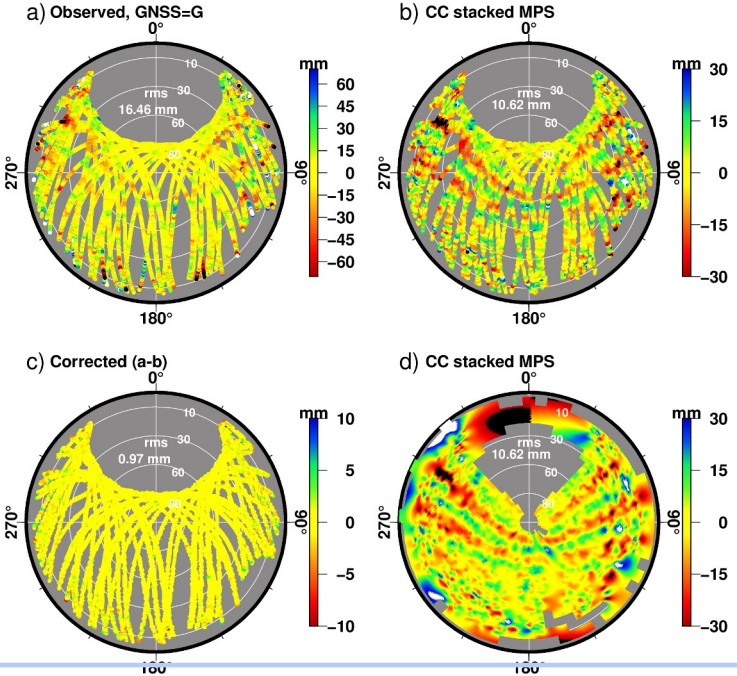

a) GPS raw post-fit residuals above the local horizon (gaps due to GPS satellite tracks) **b)** Multipath stacked map **c)** Ccorrected post-fit residuals **d)** interpolated MPS

The station is located on the roof of the white building. Power lines cross along the east-west direction with respect to the station.

Stacking of the post-fit residuals provide corrections to remove errors due to mainly MP effects as a function of elevation/azimuth

Skyplots of the post-fit residuals at ISTA and SLEE for DOY 208 during the storm for satellite PRN21 and PRN10, respectively. Note the difference in scale.

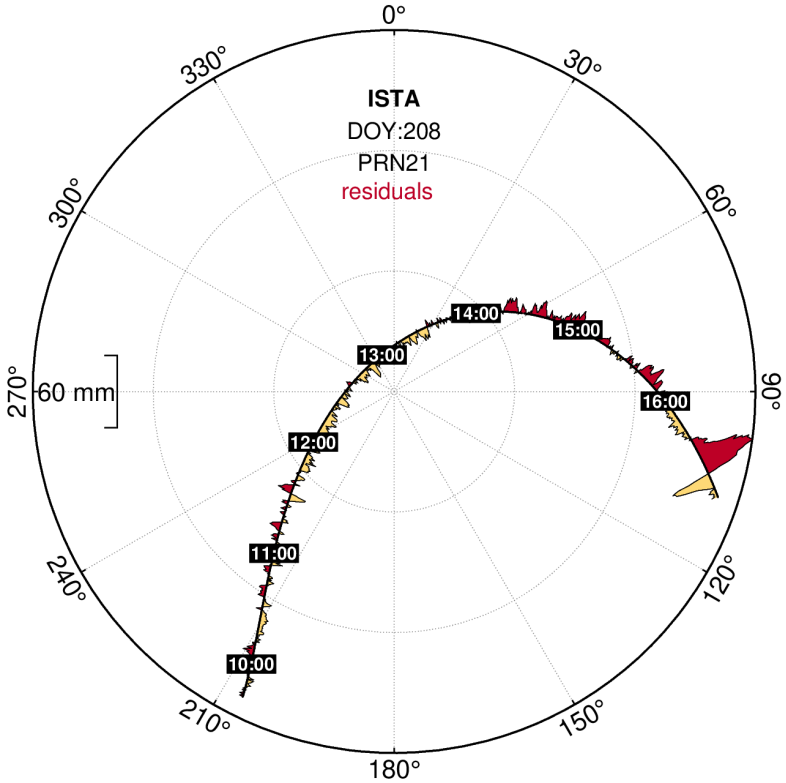

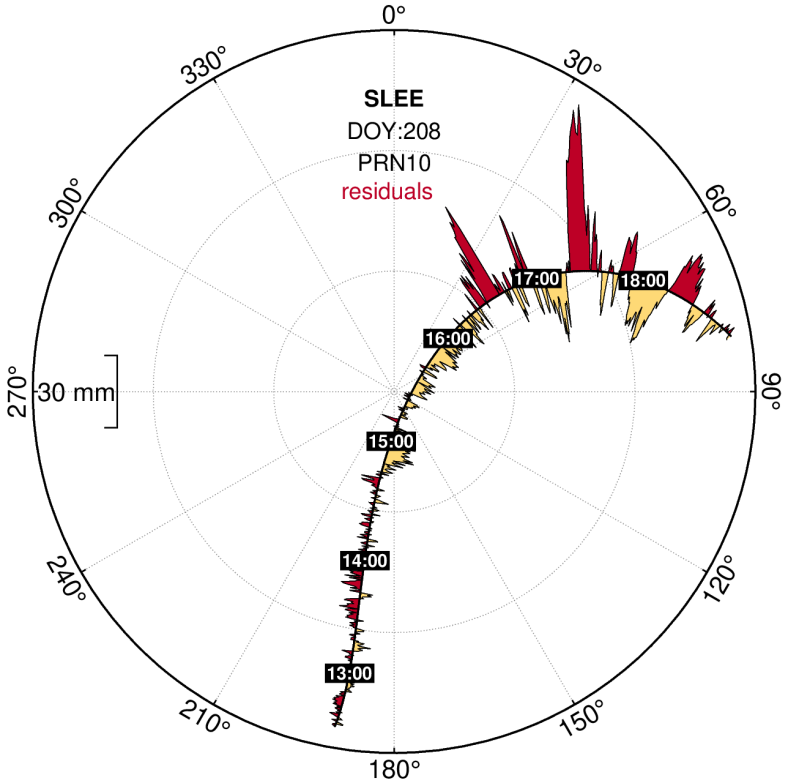

Assess impact of constraints on ZWD estimate. Test of different ZWD/GRD constraints by random walk (RW) processes

$ZWD \rightarrow 1cm \cdot h^{-1/2}$

$GRD \rightarrow 1mm \cdot h^{-1/2}$

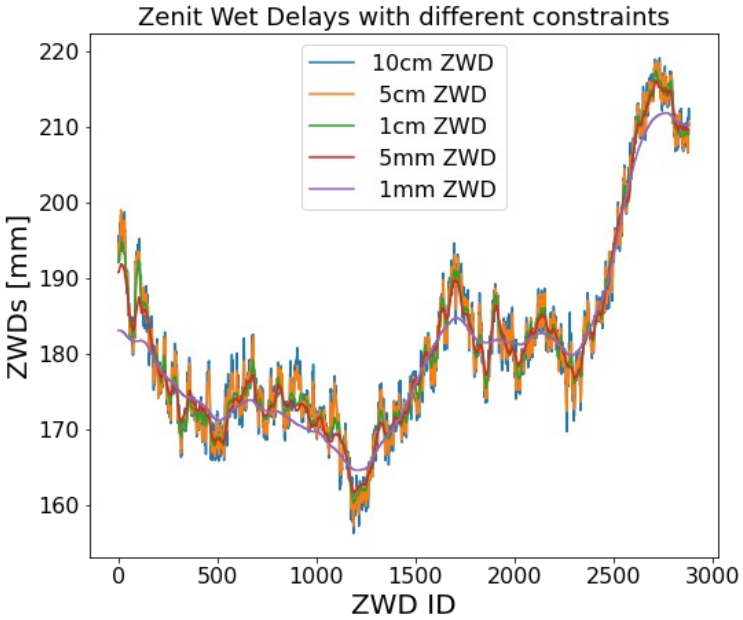

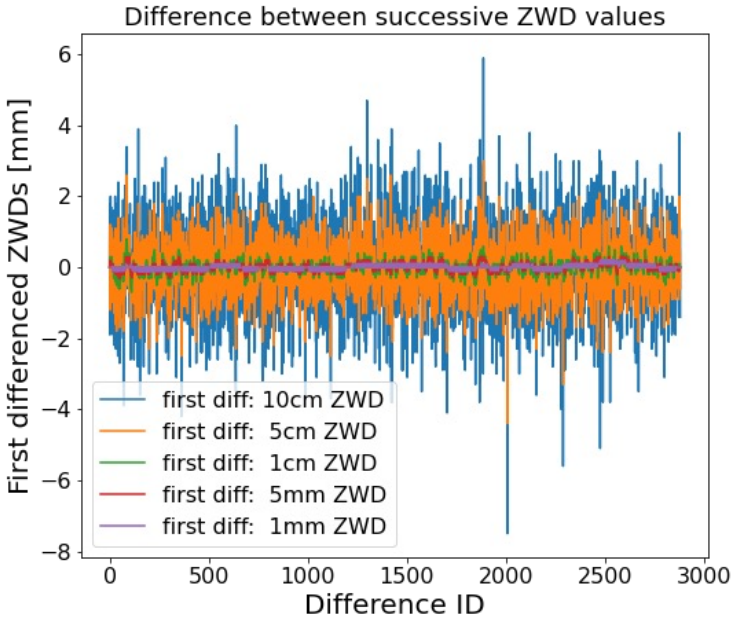

Our choice of RW constraint follows the recommendation by Selle and Desai, 2016 (minimized differences between WVR data & GPS). The first differences of our choice also show minimum while capturing the variabilities of ZWD during the storm.

Comparison of GPS-derived PWV and the global precipitation measurement (GPM) mission. Motion of water vapour can be easily spotted allowing the visualisation of the storm shape.

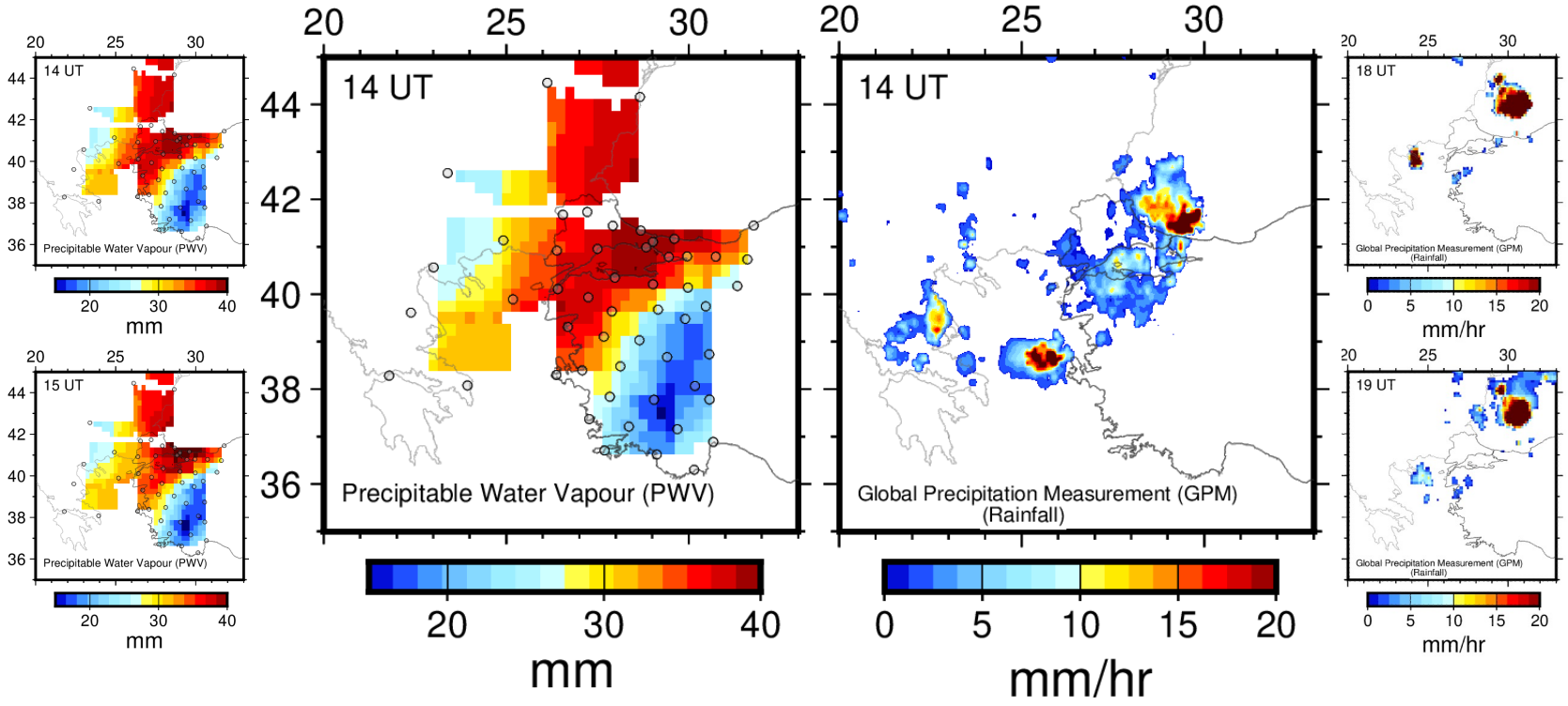

SPWV distribution in 3D vs time for all satellites and selected stations showing the SPWV to dramatically increase as the storm passes.

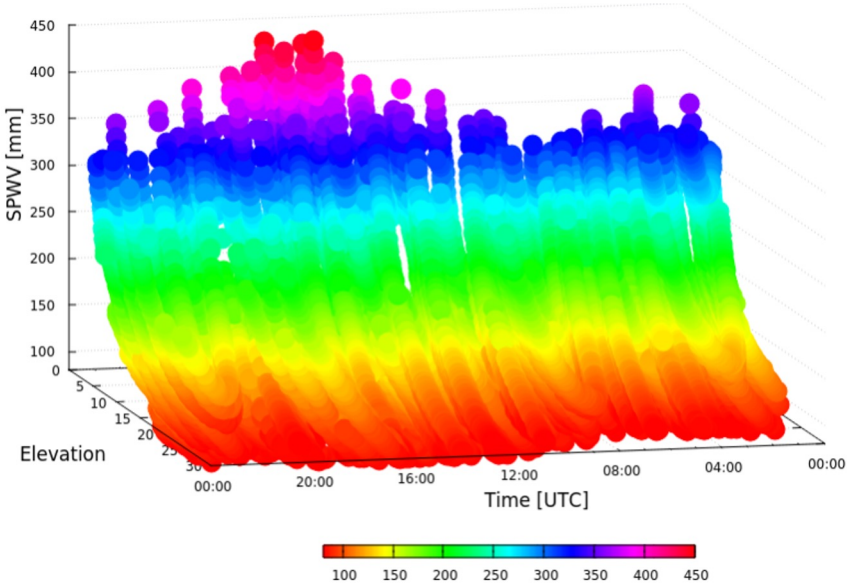

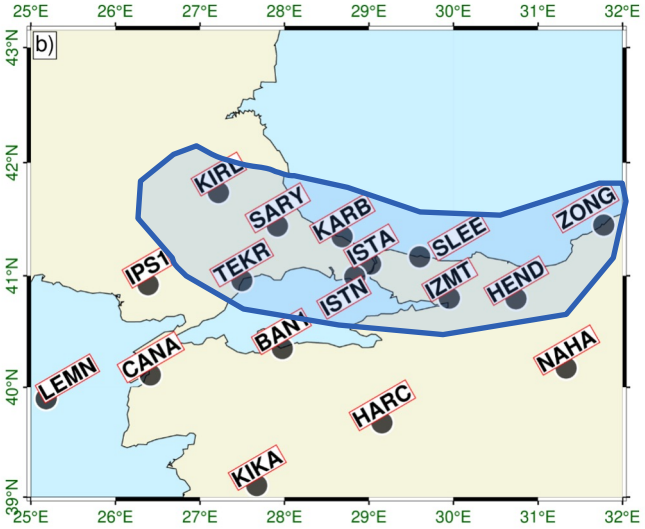

The SPWV estimates are for stations in the shaded region in the figure to the right.

Investigation of the isotropic and non-isotropic SPWV variations for PRN10 and PRN21 at SLEE and ISTA vs time.

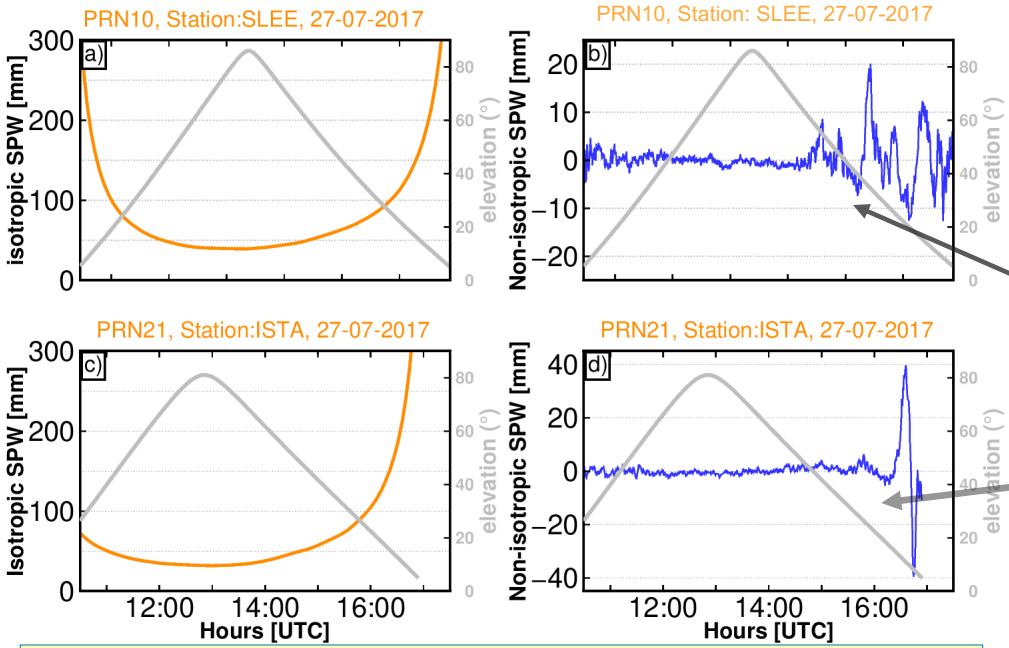

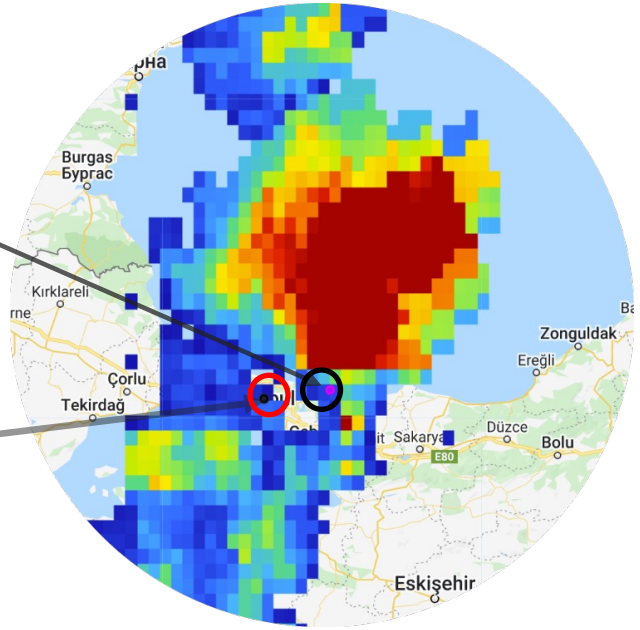

The isotropic (left) and non-isotropic (right) SPWD. For SLEE the non-isotropic contribution reaches **20**% of the isotropic component.

GPM precipitation at 17:00 UTC:

The effect of MPS on the estimate of the non-isotropic SPWV for ISTA and SARY for different satellites.

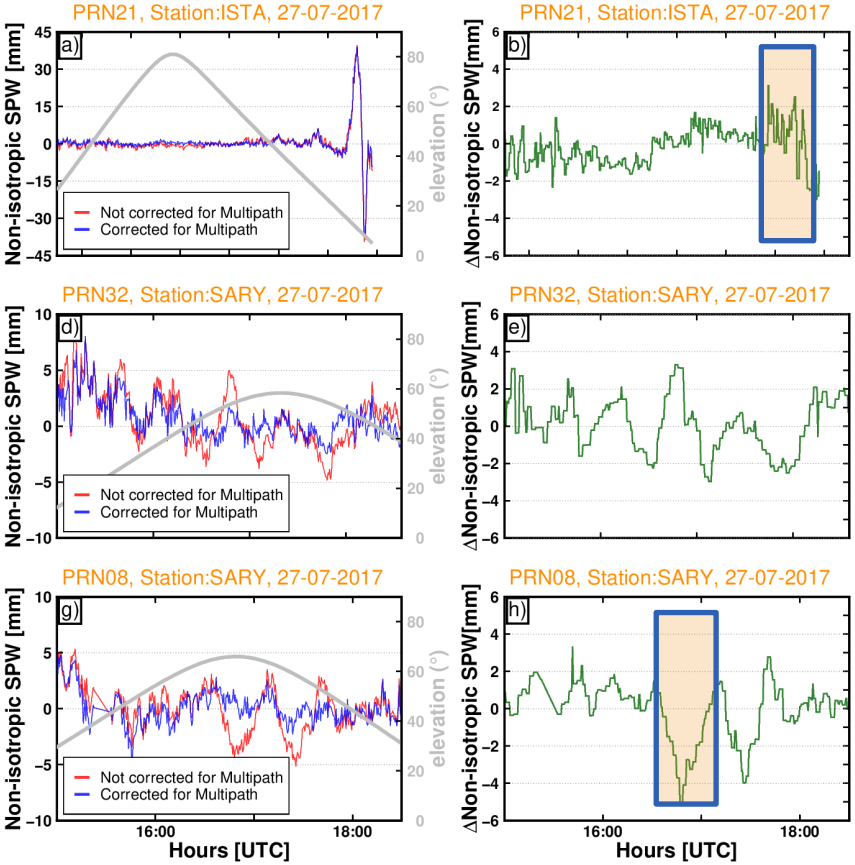

Non-isotropic (left) SPWV with MP correction (blue colour) and without MP correction (red colour) and their differences (right panels) for ISTA and SARY.

For SARY, which is adversely affected by MP, the peak variability difference can reach $5\ mm$.

Not correcting for MP at ISTA, the 3 mm variations in SPWV can be as large as 0.8 mm of equivalent PWV at 10°. For SARY, the 5 mm variations in SPWV can be as large as 4.3 mm in equivalent PWV at 60°elevation angle.

Comparison of 30s GPS SWD with ray-traced hourly ERA5 SWD.

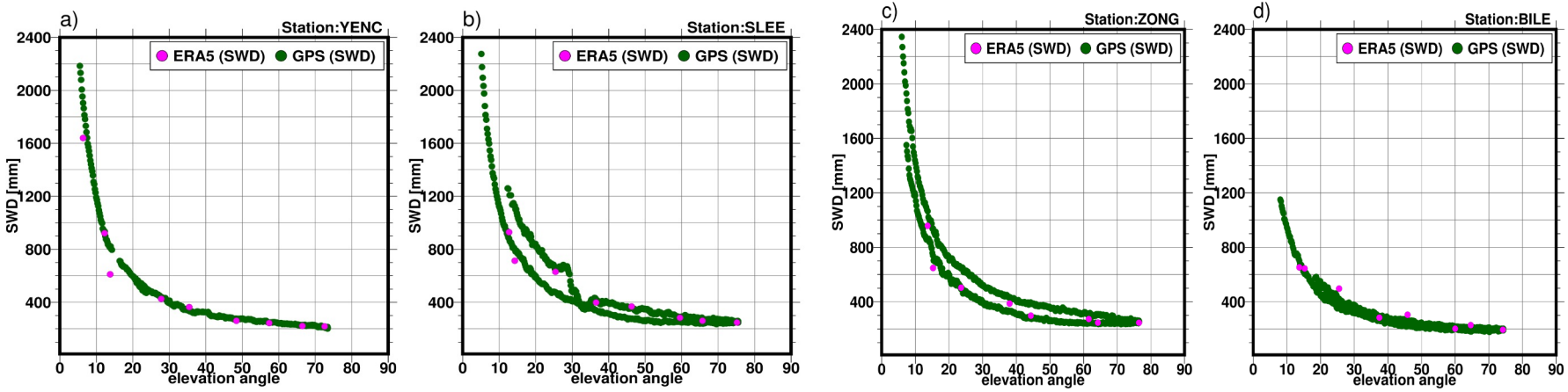

ERA5 has a coarse horizontal resolution and is unable to resolve small-scale WV features.

ERA5 STD is computed from refractivity field developed by Zus et al., Radio Sci, 49(3): 207-216

The SWD differences vs elevation angle between ERA5 and GPS solutions (for 54 stations) and all satellites show few variations between corrected and not corrected cases and are nearly equivalent.

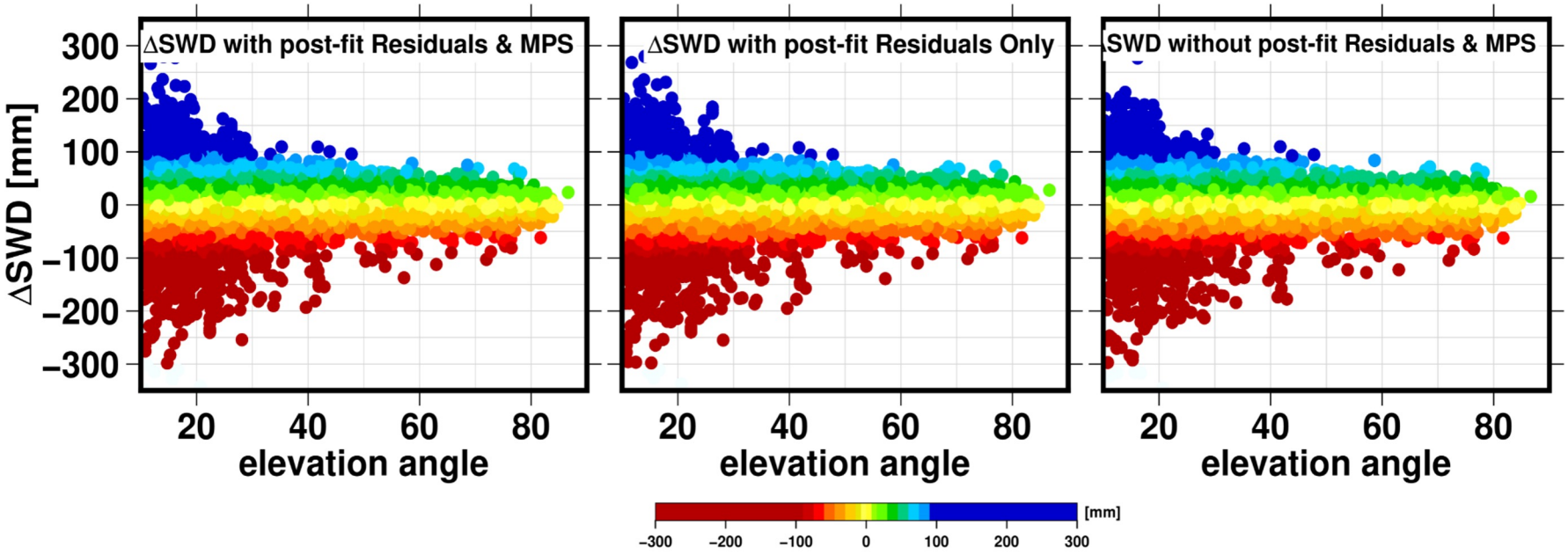

The SWD differences vs elevation angle between ERA5 and GPS solutions (for 54 stations) for PRN10 show few variations between corrected and not corrected cases and are visually nearly equivalent.

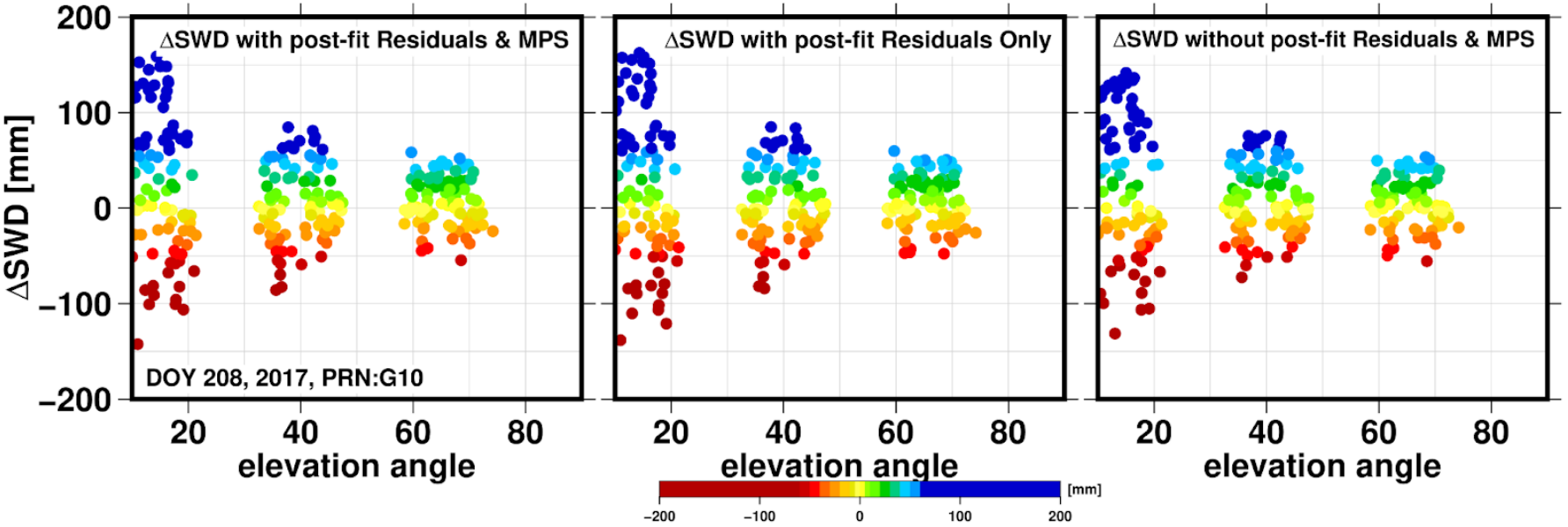

The SWD biases, RMS and standard deviations between ERA5 and GPS solutions (same epoch, elevation and azimuth) for 54 stations and corrected and not corrected cases.

SWD difference statstics [All] [mm]			
With post-fit residuals and MPS			
Comparison	Bias	RMS	SD
ERA5-GPS	1.7	55.5	55.5
With post-fit residuals			
ERA5-GPS	1.7	56.0	55.9
Without post-fit residuals and MPS			
ERA5-GPS	1.8	53.9	53.9

Comparison **for all satellites** for 24 hours during the severe weather event

SWD difference statstics [PRN10] [mm]			
With post-fit residuals and MPS			
Comparison	Bias	RMS	SD
ERA5-GPS	5.1	40.4	40.1
With post-fit residuals			
ERA5-GPS	5.8	40.6	40.3
Without post-fit residuals and MPS			
ERA5-GPS	6.7	41.3	40.9

Comparison **for one satellite (PRN10)** for 24 hours during the severe weather event

Conclusions

- The resulting non-isotropic precipitable slant wet component contribution can reach 20% of the isotropic precipitable slant wet component (equivalent PWV)
- For a station with strong MP, the peak variability can reach 5mm of non-isotropic contribution to SPWV. At 60 deg elevation angle, the variability can be as large as 4.3 mm in PWV projected to the zenith direction
- The GPS-derived SWD agrees well with the ray-traced ERA5-derived SWD but from this first comparison it seems that over 24 hours SWD for all satellites is not affected by corrections but SWD from individual satellites can be.
- Tests show that MPS maps contain unmodelled PCO/PCV errors and that the maps can absorb PCO/PCV values of uncalibrated antennas, i.e. low-cost antennas (not shown)